Journal of Catalysis 266 (2009) 106–119

Contents lists available at ScienceDirect

Journal of Catalysis

journal homepage: www.elsevier.com/locate/jcat

Experimental and kinetic study of NO oxidation on model Pt catalysts

Divesh Bhatia [a], Robert W. McCabe [b], Michael P. Harold [a,*], Vemuri Balakotaiah [a,*]

[a] Dept. of Chemical and Biomolecular Engineering, University of Houston, 4800 Calhoun Road, Houston, TX 77204, United States
[b] Research and Innovation Center, Ford Motor Company, Dearborn, MI 48124, United States

ARTICLE INFO

Article history:
Received 16 March 2009
Revised 27 May 2009
Accepted 28 May 2009
Available online 9 July 2009

Keywords:
NO oxidation
NO_2 decomposition
Poisoning
Deactivation
Storage
Kinetics
Transient
Modeling
NSR

ABSTRACT

Modeling and experimental studies on model Pt/Al_2O_3 and $Pt/BaO/Al_2O_3$ catalysts are performed to elucidate the kinetics of NO oxidation, which is a key step during the lean phase of NO_x trap operation. Experiments show that a steady-state is never truly achieved during NO oxidation; a continuous decrease in the reaction rate with time is observed on both the catalysts. This decrease is distinct from and beyond the prompt inhibition of the NO oxidation reaction observed with NO_2 in the feed or product. NO oxidation carried out after catalyst pretreatments with H_2, O_2, and NO_2 indicates that NO_2 is responsible for the deactivation while NO_2 storage plays a negligible role. Experiments with NO_2 as the feed elucidate its role in the production of NO, either by storage or by decomposition, for a wide range of temperatures. The highly oxidizing nature of NO_2 suggests that the Pt surface could be covered with oxygen, either as chemisorbed O or as Pt oxides, which results in slow poisoning of the catalyst. Microkinetic analysis of the NO oxidation reaction shows O_2 adsorption as the rate-determining step and predominant surface species to be adsorbed NO and O. Based on the microkinetic studies, a global kinetic model is proposed which includes the inhibiting effect of NO_2 on the NO oxidation reaction. The importance of including coverage of NO in the global model at low temperatures is shown, which is neglected in the current literature global models. The model predicts the experimental observations for a wide range of temperatures within acceptable error limits. However, prediction of the transient data requires modeling of NO_2 storage, decomposition and the complex NO_2 inhibition chemistry in addition to other surface reactions.

1. Introduction

Lean burn gasoline and diesel vehicles are gaining attention because of their better fuel economy than stoichiometric gasoline counterparts. However, the presence of excess O_2 in the exhaust makes the three-way or diesel oxidation catalysts much less effective in reducing NO_x. This poses a challenge in meeting the stringent future NO_x emission standards while keeping the catalyst costs low. Several NO_x reduction technologies under development in the previous years have now been commercialized, including selective catalytic reduction (SCR) with NH_3 or urea, SCR with hydrocarbons, and NO_x storage and reduction (NSR). The focus of the current work is NSR technology, which is being used currently in some light duty diesel passenger cars and trucks.

NSR technology consists of two cyclic steps that occur on a lean NO_x trap (LNT) catalyst: NO_x storage during the lean phase and reduction during the rich phase. The LNT contains a bifunctional catalyst comprising precious metals (Pt, Pd, and Rh), which are used for NO oxidation and reduction, and alkaline earth or alkali metals (Ba, K, etc.) in the form of carbonates or oxides which provide the storage function. The main aim of NSR technology is to achieve a high NO_x conversion selectively to N_2 while minimizing the fuel penalty. Since the operation of a NSR catalyst is a complex process involving NO oxidation, storage and reduction, we limit our attention to the lean phase in this work.

The lean NO_x trap (LNT) catalyst readily stores NO_2 as compared to NO [1,2]. For this reason, NO should be oxidized to NO_2 to achieve an acceptable level of NO_x storage. It has been shown that placing a Pt/Al_2O_3 catalyst before a $Pt/BaO/Al_2O_3$ catalyst results in an increase in the NO_x storage capacity of the overall system [3]. This is a result of the formation of NO_2 over the Pt/Al_2O_3 catalyst, which then stores on BaO downstream. On the other hand, physical mixtures of Pt/Al_2O_3 and BaO/Al_2O_3 are less effective than co-impregnated $Pt/BaO/Al_2O_3$ catalysts [4,5]. Thus, the close coupling between Pt, where NO oxidation occurs, and BaO, where storage occurs, is paramount. The focus of the current study is the NO oxidation reaction over Pt/Al_2O_3 and $Pt/BaO/Al_2O_3$ catalysts since the oxidation reaction is crucial for the efficient operation of a NO_x trap during the lean phase.

Experimental studies of NO oxidation over Pt-based catalysts have been performed by a number of research groups [6–11]. Modeling studies to elucidate the steady-state and transient kinetics of the NO oxidation reaction have also been a topic of active research [3,7,8,11–13]. Olsson et al. [3] studied the kinetics of NO oxidation

* Corresponding authors. Fax: +1 713 743 4323.
E-mail addresses: mharold@uh.edu (M.P. Harold), bala@uh.edu (V. Balakotaiah).

0021-9517/$ - see front matter © 2009 Elsevier Inc. All rights reserved.
doi:10.1016/j.jcat.2009.05.020

Nomenclature

a	side length of square channel (m)
A_{bi}	reverse pre-exponential factor for step i (mol/m^3 washcoat s)
A_{fi}	forward pre-exponential factor for step i (mol/m^3 washcoat s)
A_Ω	channel cross-sectional area open to flow (m^2)
c_j	concentration of species j (mol/m^3)
c_{Tm}	total molar concentration (mol/m^3)
C_{pf}	specific heat capacity of fluid phase (J/kg K)
D_{jm}	diffusivity of species j in the gas phase (m^2/s)
D_{je}	diffusivity of species j in the washcoat (m^2/s)
E_{bi}	reverse activation energy of step i (kJ/mol)
E_{fi}	forward activation energy of step i (kJ/mol)
GHSV	gas hourly space velocity (h^{-1})
h_f	heat transfer coefficient (W/m^2 K)
k_{bi}	reverse rate constant for step i (mol/m^3 washcoat s)
$k_c(j,z)$	mass transfer coefficient of species j at axial position z (m/s)
k_{fi}	forward rate constant for step i (mol/m^3 washcoat s)
k_s	thermal conductivity of support (W/m K)
k_w	effective thermal conductivity of solid (W/m K)
k_{wc}	thermal conductivity of washcoat (W/m K)
K_{eq}	equilibrium constant for NO oxidation reaction
K_i	equilibrium constant of microkinetic step i
L	length of the monolith sample (m)
N_s	number of species adsorbed on the catalyst surface
P_Ω	channel perimeter open to flow (m)
Pe_h	Peclet heat number
r	number of microkinetic reactions
R	universal gas constant (kJ/mol K)
$R_{ad,\,j}$	rate of adsorption of species j (mol/m^3 washcoat s)
$R_{c,\,j}$	rate of consumption of surface species j (mol/m^3 washcoat s)
$R_{des,\,j}$	rate of desorption of species j (mol/m^3 washcoat s)
$R_{g,\,j}$	rate of generation of surface species j (mol/m^3 washcoat s)
R_v	reaction rate (mol/m^3 washcoat s)
R_{v,NO_ox}	predicted rate of NO oxidation reaction (mol/m^3 washcoat s)
R_Ω	effective transverse length scale (m)
t_c	characteristic convection time (s)
t_d	characteristic transverse diffusion time (s)
t_R	characteristic reaction time (s)
T_m	cup-mixing fluid temperature (K)
TOF	turnover frequency (moles NO_2 formed/moles exposed Pt s)
T_s	catalyst temperature (K)
$\bar{u}$	average gas velocity in the gas phase (m/s)
υ	inlet volumetric flow rate to the reactor (L/min)
V_c	catalyst volume (m^3)
X_j	mole fraction of species j
X_{jm}	dimensionless cup-mixing concentration of species j in fluid
$\widehat{X}_j$	mole fraction of species j in the washcoat
y	transverse coordinate (m)
z	axial coordinate (m)

Greek letters

δ_c	washcoat thickness (m)
δ_s	half thickness of support (m)
δ_w	effective wall thickness (m)
$\Delta H_{R,l}$	heat of reaction l (kJ/mol)
ΔT_{ad}	adiabatic temperature rise (K)
ε_w	washcoat porosity
Ψ	Weisz modulus
ϑ_j	stoichiometric coefficient of species j in the reaction (negative for reactant)
ρ_f	density of fluid (kg/m^3)
θ_j	fractional surface coverage of adsorbed species j
θ_v	fractional coverage of vacant sites

Subscripts

in	inlet
out	outlet
avg	average
s	washcoat-fluid interface

on Pt/Al_2O_3 and $Pt/BaO/Al_2O_3$ and proposed a Langmuir–Hinshelwood mechanism to predict the experimental results. Their analysis showed that oxygen desorption is the rate-limiting step for NO_2 decomposition to NO on Pt/Al_2O_3. Using XPS and flow reactor experiments, Olsson and Fridell [6] explained the lower activity of $Pt/BaO/Al_2O_3$ compared to Pt/Al_2O_3 as being due to a higher amount of PtO_2 formation on $Pt/BaO/Al_2O_3$. Muncrief et al. [8] reported a similar lower activity for $Pt/BaO/Al_2O_3$ compared to Pt/Al_2O_3 powders. They obtained a satisfactory fit of the conversion vs. temperature data using a pseudo first order with respect to NO. However, the effect of NO_2 was not studied and therefore the model did not include NO_2 concentration in the rate expression for the forward reaction. Marques et al. [7] performed steady-state NO oxidation experiments on Pt/SiO_2 and $Pt/CeZrO_2$ and found a positive-order dependence of the NO oxidation rate in NO and O_2. They too did not study the effect of NO_2. Mulla et al. [9] found that NO_2 inhibited the NO oxidation reaction and determined the oxidation reaction to have a negative order dependence with respect to NO_2 (-0.92). They proposed non-dissociative O_2 adsorption as the rate-limiting step and derived a rate expression for NO oxidation which predicted a negative order in NO_2. The reaction rate expression considered the reverse reaction, i.e. NO_2 decomposition to NO and O_2. However, like in the other studies, NO_2 decomposition was not studied independently.

Since NO oxidation and NO_x storage occur simultaneously on a LNT catalyst, it is challenging to study the oxidation reaction in isolation. Hence, we perform experiments with an inlet feed of NO_2 for various temperatures to study the NO_x storage and decomposition independent of NO oxidation. Experiments are also performed on a Pt/Al_2O_3 catalyst to minimize any NO_x storage effects during the NO oxidation. Transient NO oxidation experiments after various catalyst pretreatments are done on Pt/Al_2O_3 to investigate the cause of an observed activity decrease with time. The inhibitive effect of NO_2 on the NO oxidation reaction is evaluated by performing NO oxidation experiments for various NO_2 concentrations. The rate-limiting step and the predominant surface species are obtained with a microkinetic analysis of the NO oxidation and NO_2 decomposition reaction systems. Based on these studies, an improved global kinetic model is developed that predicts key trends in the data. To this end, limitations of the literature models are discussed.

2. Experimental

2.1. Catalyst samples

Pt/Al_2O_3 and $Pt/BaO/Al_2O_3$ samples used in this study were provided by BASF Catalysts LLC (Iselin, NJ) in monolithic form.

Table 1
Composition and properties of catalysts used in the present work.

Sample	Pt loading (g/ft^3)	Pt (wt%)	BaO (wt%)	Pt dispersion (%)	Pt area (m^2/g washcoat)	Pt particle size (nm)
B4	120	3.71	16	34.7	3.18	3.26
A3	70	2.63	0	20.3	2.21	5.59

Cylindrical cores were cut to obtain the catalyst samples of the desired length and diameter. The lengths of the Pt/Al_2O_3 and $Pt/BaO/Al_2O_3$ samples were 1.5 cm and 1.3 cm, respectively. Both samples had a cell density of 62 channels/cm^2 (400 cpi) and a diameter of ~1.7 cm. However, the total number of channels for Pt/Al_2O_3 and $Pt/BaO/Al_2O_3$ samples was 131 and 127, respectively, because of the non-uniform cutting of the monolith core close to the outer edges. The weights of Pt/Al_2O_3 and $Pt/BaO/Al_2O_3$ samples used were 1.87 g and 1.57 g, respectively. The composition and properties of the catalyst samples used in this study were provided by BASF Catalysts LLC (Iselin, NJ) and are given in Table 1. B4 in Table 1 denotes the $Pt/BaO/Al_2O_3$ catalyst and A3 denotes the Pt/Al_2O_3 catalyst. The preparation method of each catalyst is described by Clayton et al. [14].

2.2. Monolith properties

The monolith sample (B4) was observed using an optical microscope for various magnifications to measure the catalyst dimensions. A schematic of the cross-sectional view of the monolith channel is shown in Fig. 1. The shaded region represents the washcoat cross-section, whereas the square of side length 'a' represents the area for fluid flow. The outermost unshaded region represents the support, which has a thickness equal to $2\delta_s$. The width of the flow region (a) and thickness of the cordierite support were determined using the microscopic measurements, whereas the average thickness of the washcoat (δ_c) was calculated using

$$\delta_c = \delta_w - \delta_s \tag{2.1}$$

Here, δ_w represents the effective thickness of the wall (=Total wall thickness/2). The measured dimensions of the monolith sample are given in Table 2.

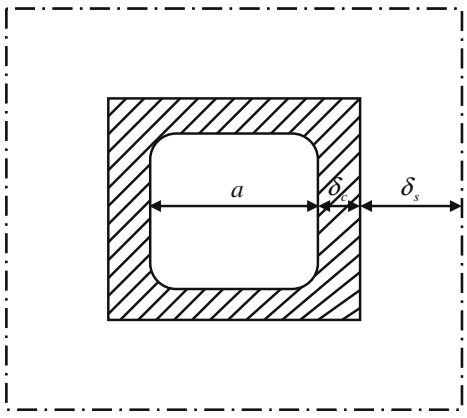

Fig. 1. Schematic diagram illustrating the cross-section of a single monolith channel.

Table 2
Measured values of the monolith and washcoat dimensions.

Monolith dimension	Value (m)
a	1.099×10^{-3}
δ_s	8.85×10^{-5}
δ_c	1.45×10^{-5}

2.3. Flow reactor set-up

The experimental set-up used in this study is shown in Fig. 2. Various gases were fed to the atmospheric pressure reactor from gas cylinders (Airgas) and the flow rates were metered by mass flow controllers (Matheson Gas Products). All the gas lines were heated to prevent water condensation and NH_3 adsorption. The catalyst sample was placed in a quartz tube of 11/16″ inner diameter, which itself was placed horizontally in a furnace (Lindberg Blue). The monoliths were wrapped with Fiberfrax® ceramic paper to prevent gas bypassing between the sample periphery and tube wall. The catalyst and inlet gas temperatures were measured by *K*-type stainless steel-sheathed thermocouples. The thermocouple used to measure the catalyst temperature was positioned in a monolith channel at the approximate midpoint of the monolith (axial and radial), whereas the thermocouple to measure the inlet gas temperature was positioned 2″ from the front of the sample. Data were recorded on a PC using the software PDaq View (Iotech Inc.). The effluent from the flow reactor was analyzed using a FT-IR spectrometer (MKS Model 2030) and the gas concentrations were recorded on another PC. The species monitored by the FT-IR included NO, NO_2, NH_3, N_2O, H_2O, and CO_2. The sampling frequency was 1 Hz for both the FT-IR analyzer and the temperature measurements. Unless otherwise mentioned, the total gas volumetric flow rate (=υ) was 3 L/min, which corresponds to a gas hourly space velocity (GHSV = υ/V_c) of 4.9×10^4 h^{-1} and 5.72×10^4 h^{-1} for samples A3 and B4, respectively. The carrier gas in all the experiments was N_2.

2.4. Catalyst aging

An aging protocol was used to stabilize the catalytic activity so that the experiments could be compared without large activity changes over prolonged periods of time on stream. This de-greening protocol consisted of flowing a net-reducing mixture over the sample for 10 min at an inlet temperature of 600 °C. The total flow rate was 2.5 L/min and the composition of the inlet gas was as follows: 5% CO_2, 5% H_2O, 1.5% CO, 0.5% H_2, and 88% N_2.

2.5. Steady-state experiments

The steady-state NO oxidation experiments were performed by flowing N_2 to the reactor followed by the reactant gases. The inlet gas temperature was maintained at the desired value by adjusting the set point of the furnace. The typical time to achieve a steady-state varied from a few minutes (30–60 min) for low and high temperatures (T_s < 200 °C and T_s > 350 °C) to as long as a few hours for the intermediate temperatures. As will be discussed later, a "true" steady-state is not achieved during the NO oxidation experiments, especially at the intermediate temperatures. Hence, pseudo steady-state data have been reported in the present work.

2.6. Transient experiments

Transient NO oxidation and NO_2 storage and decomposition experiments were done to investigate the decrease in reaction rates with time. The catalyst was first reduced with 5% H_2 (balance N_2) at an inlet temperature of 485 °C for 2 h before performing the transient experiments. This was done to react away any adsorbed

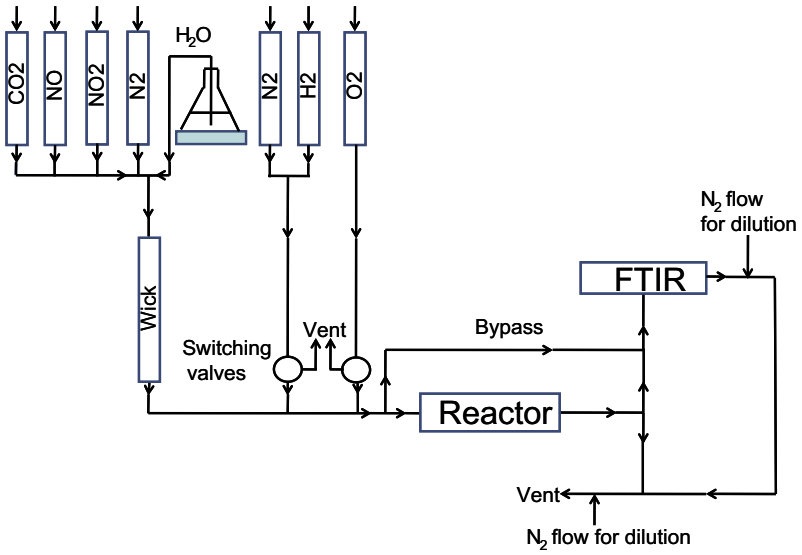

Fig. 2. Experimental set-up.

N or O species. For the pretreatment experiments, the catalyst reduction was followed by switching off the H_2 and reducing the inlet temperature to 192 °C. Then the desired pretreatment gas (5% O_2 for O_2 pretreatment or 524 ppm NO_2 for NO_2 pretreatment) was passed over the Pt/Al_2O_3 catalyst for 1 h, after which the flow was switched to pure N_2 for 10 min to remove any loosely bound O or N species from the surface. This was followed by flowing 500 ppm NO and 5% O_2 over the catalyst for 1 h during which the product concentration was monitored with time. For the reductive pretreatment experiment, the NO oxidation experiment involving a feed of 500 ppm NO and 5% O_2 was carried out just after bringing the inlet temperature down to 192 °C following the catalyst reduction.

3. Modeling and simulations

3.1. Reactor model

Modeling studies were aimed at predicting the steady-state experimental results for NO oxidation over a range of temperatures and feed compositions. A one-dimensional two-phase model is used, the details of which have been reported elsewhere [15]. For completeness, the model equations used in the current work are given in Table 3. The model equations consist of species and energy balances in the fluid and solid phases. Adiabatic boundary conditions are used for the solid energy balance, whereas inlet conditions are specified for the concentration and temperature in the fluid phase. Effective heat and mass transfer coefficients are used to account for the transverse gradients. The non-isothermal behavior of the system is taken into account in the current model by considering the heat of reaction of the individual reactions. The following assumptions are made: (i) constant physical properties with temperature and composition, (ii) steady-state operation, (iii) adiabatic operation, (iv) laminar flow, and (v) negligible washcoat diffusional limitations. Finally, the value of $\delta_w k_w$ given in Table 3 was evaluated using $\delta_w k_w = \delta_c k_{wc} + \delta_s k_s$, where k_{wc} and k_s are the thermal conductivities of the washcoat and support, respectively.

Table 3
Steady-state model equations obtained by neglecting diffusion in the washcoat [15].

$$\bar{u}\frac{dX_{jm}}{dz} = -\frac{k_c(j,z)}{R_\Omega}(X_{jm} - X_{js})$$

$$X_{jm} - X_{js} + \frac{\delta_c}{c_{Tm}k_c(j,z)}\vartheta_j R_v(T_s, \underline{X_s}) = 0$$

$$\rho_f C_{pf}\bar{u}\frac{dT_m}{dz} = -\frac{h_f(z)}{R_\Omega}(T_m - T_s)$$

$$\delta_w k_w \frac{d^2T_s}{dz^2} - h_f(z)(T_s - T_m) - \delta_c \Delta H_R R_v(T_s, \underline{X_s}) = 0$$

Boundary conditions:
$X_{jm} = X_{jm,in} \quad and \quad T_m = T_{m,in} \quad at \quad z = 0$
$\frac{dT_s}{dz} = 0 at z = 0, L$

Table 4
Steady-state model equations for analyzing microkinetic reaction scheme [15].

$$X_{jm,in} - X_{jm} - \frac{k_c(j)L}{\bar{u}R_\Omega}(X_{jm} - X_{js}) = 0$$

$$X_{jm} - X_{js} + \frac{\delta_c}{c_{Tm}k_c(j)}(R_{des,j} - R_{ad,j}) = 0$$

$$T_{m,in} - T_m - \frac{h_f L}{\bar{u}\rho_f C_{pf} R_\Omega}(T_m - T_s) = 0$$

$$T_m - T_s - \frac{\delta_c}{h_f}\sum_{l=1}^{r}\Delta H_{R,l}R_{v,l}(T_s, \underline{X_s}) = 0$$

$$\sum_j (R_{c,j} - R_{g,j}) = 0$$

$$\sum_{j=1}^{N_s}\theta_j + \theta_v = 1$$

Table 5
Steady-state model equations obtained by considering diffusional limitations in the washcoat.

$$\bar{u}\frac{dX_{jm}}{dz} = \frac{D_{je}}{R_\Omega}\frac{\partial \widehat{X}_j}{\partial y}\bigg|_{y=0}$$

$$c_{Tm}D_{je}\frac{\partial^2 \widehat{X}_j}{\partial y^2} + \vartheta_j R_v(T_s, \widehat{\underline{X}}) = 0$$

$$\rho_f C_{pf}\bar{u}\frac{dT_m}{dz} = -\frac{h_f(z)}{R_\Omega}(T_m - T_s)$$

$$\delta_w k_w \frac{d^2T_s}{dz^2} - h_f(z)(T_s - T_m) - \Delta H_R \int_0^{\delta_c} R_v(T_s, \widehat{\underline{X}})dy = 0$$

Boundary conditions:
$\widehat{X}_j = X_{js} \quad at \quad y = 0$
$\frac{\partial \widehat{X}_j}{\partial y} = 0 \quad at \quad y = \delta_c$

Table 6
Values of physical properties and other parameters used in the simulations.

Parameter	Parameter value
$\bar{u}$	0.316 m/s
L	0.0154 m
R_Ω	2.75×10^{-4} m
ρ_f	1.067 kg/m^3
C_{pf}	1009 J/kg K
$D_{NO,m}$	4.57×10^{-5} m^2/s
$D_{O_2,m}$	4.57×10^{-5} m^2/s
$D_{NO_2,m}$	3.42×10^{-5} m^2/s
ΔH_R	−57.2 kJ/mol
k_{wc}	20 W/m K
k_s	2.5 W/m K

To analyze the microkinetic reaction scheme for studying NO oxidation, a short monolith reactor model was used [15]; the corresponding equations are given in Table 4. The model equations given in Tables 3 and 4 are applicable when diffusional limitations in the washcoat are assumed to be absent. To study the effect of diffusional processes in the washcoat on the simulation results, diffusion-reaction equations in the washcoat were considered and the model equations are given in Table 5. The boundary conditions for the solid temperature, fluid phase temperature, and concentration are the same as for the previous model (Table 3).

3.2. Numerical simulations

The values of physical properties and other parameters used in the simulations are given in Table 6. The diffusivity of gas species in the fluid phase was calculated using Lennard–Jones potentials. The position-dependent mass transfer coefficients and heat transfer coefficient were evaluated for a channel of square cross-section using an expression developed by Ramanathan and Balakotaiah [16]. To solve the one-dimensional two-phase model, the differential equations representing mass and energy balances were discretized in the axial direction to get a set of non-linear equations. These equations were solved using the arc-length method [17], which consists of varying both the state variables and the bifurcation parameter with the arc-length, thus making the bifurcation parameter another unknown in the system.

4. Results and discussion

4.1. Pt/BaO/Al_2O_3

4.1.1. Steady-state experiments

Steady-state NO oxidation experiments were performed with an inlet NO concentration of 528 ppm and excess O_2 (5%) on the Pt/BaO/Al_2O_3 monolith catalyst (B4). Fig. 3 shows the dependence of steady-state and equilibrium NO conversion on the catalyst temperature for temperatures ranging between 90 °C and 500 °C. The dependence of NO equilibrium conversion on the catalyst temperature was determined using temperature-dependent specific heat capacities. It is observed that the steady-state NO conversion goes through a maximum at a temperature of about 350 °C. The maximum is expected for an exothermic reversible reaction: At temperatures lower than 350 °C, the conversion is limited by kinetics and mass transfer, whereas at higher temperatures, the conversion is limited by reaction equilibrium. Similar results were reported by Epling et al. [2] and Muncrief et al. [8]. A maximum in NO conversion at 372 °C on Pt/SiO_2 was also reported by Marques et al. [7] during temperature programmed surface NO oxidation reaction. Olsson et al. [3] reported a maximum in NO conversion on Pt/Al_2O_3 and Pt/BaO/Al_2O_3 catalysts at 390 °C, when 600 ppm NO was oxidized in excess O_2 (8%). Thus, the NO oxidation steady-state results are consistent with those already reported in the literature.

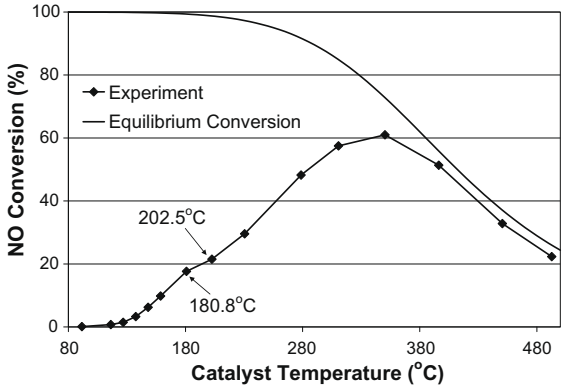

Fig. 3. Variation of steady-state NO conversion with catalyst temperature during NO oxidation on Pt/BaO/Al_2O_3 catalyst (inlet NO = 528 ppm, O_2 = 5%).

A comparison of the characteristic diffusion times, convection times, and reaction times provides insight into the rate-controlling process over the range of operating conditions. The characteristic transverse diffusion time (t_d), convection time (t_c), and reaction time (t_R) are defined as R_Ω^2/D_{jm}, $L/\bar{u}$, and $c_{NO,s}\varepsilon_w/R_v$, respectively. Here, R_Ω denotes the effective transverse diffusion length scale ($R_\Omega = A_\Omega/P_\Omega$; A_Ω = channel cross-sectional area open to flow; P_Ω = channel perimeter open to flow), D_{jm} denotes the diffusivity of species j in the gas phase, L is the length of the monolith, $\bar{u}$ is the average gas velocity, $c_{NO,s}$ is the NO concentration at the fluid-washcoat interface, ε_w is the porosity of the washcoat, and R_v is the reaction rate (based on unit washcoat volume). The surface concentrations were evaluated using the steady-state mole balance

$$\bar{u}(c_{j,in} - c_{j,out}) = \frac{k_c(j,L)L}{R_\Omega}(c_{j,avg} - c_{j,s}) \tag{4.1}$$

where the subscripts such as *in*, *out*, *avg*, and *s* refer to the inlet, outlet, average, and fluid-washcoat interface, respectively. The mass transfer coefficient of species j at the exit of the reactor, $k_c(j,L)$, was evaluated using the asymptotic Sherwood number (3.608) for a channel of square cross-section. It was shown that for the conditions used in the NO oxidation experiments, fully developed flow would be established over the final 94% of the monolith length [16]. Hence, the axial variation of the mass transfer coefficients with monolith length was neglected in the calculation of concentration at the fluid-washcoat interface. The diffusional limitations in the washcoat were evaluated by calculating the Weisz modulus, Ψ, defined as

$$\Psi = \frac{R_v \delta_c^2}{D_{NO,e} c_{NO,s}} \tag{4.2}$$

where $D_{NO,e}$ is the diffusivity of NO in the washcoat, which was calculated at 100 °C using an empirical correlation given by Mukadi and Hayes [18]. For the conditions used in NO oxidation experiments, i.e. L = 1.32 cm, R_Ω = 275 μm, $D_{NO,m} = 3.03 \times 10^{-5}$ m^2/s (evaluated at 100 °C), $\bar{u} = 0.326$ m/s, and $X_{NO,in}$ = 528 ppm, the characteristic reaction time (t_R) was estimated to exceed the transverse diffusion time (t_d) at temperatures below 200 °C, suggesting that the external mass transfer resistance was negligible. Also, the Weisz modulus was less than unity for the same temperature range, hence confirming the absence of diffusional limitations in the washcoat. Thus the data obtained below 200 °C represent the intrinsic kinetics of the NO + O_2 reaction system. The variation of solid and fluid temperature in the axial direction is expected to be negligible because of the low values of adiabatic temperature rise (ΔT_{ad}) and the heat Peclet number (Pe_h), which are defined as follows

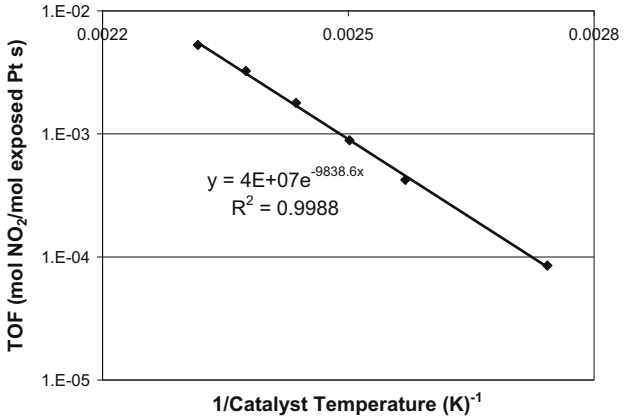

Fig. 4. Variation of NO_2 turnover frequency with inverse of catalyst temperature during NO oxidation reaction on $Pt/BaO/Al_2O_3$ catalyst (inlet NO = 528 ppm, O_2 = 5%).

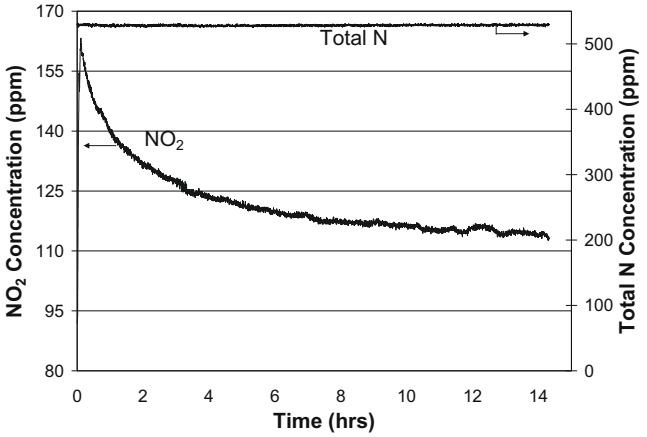

Fig. 5. Transient NO_2 concentration profile and concentration of total outlet N over $Pt/BaO/Al_2O_3$ catalyst (inlet NO = 528 ppm, O_2 = 5%, catalyst temperature = 202.5 °C).

$$\Delta T_{ad} = \frac{(-\Delta H_R)c_{NO,in}}{\rho_f C_{pf}} \tag{4.3}$$

$$Pe_h = \frac{\bar{u}L\rho_f C_{pf} R_\Omega}{(\delta_c k_{wc} + \delta_s k_s)} \tag{4.4}$$

The values of adiabatic temperature rise and Peclet heat number [19] were calculated to be 0.72 °C and 2.49, respectively. In Eq. (4.3), ΔH_R is the heat of reaction, ρ_f is the density of the fluid phase, and C_{pf} represents the specific heat capacity of the fluid phase.

The overall activation energy of the NO oxidation reaction was determined over the temperature range for which the NO conversion was less than 20%, as shown in Fig. 4. The activation energy was estimated to be 81.8 kJ/mol. Muncrief et al. [8] reported an activation energy of 36 kJ/mol for a $Pt/BaO/Al_2O_3$ powder catalyst. A potential reason for the difference between the previous studies and the current one is the difference in the catalysts used in the two studies. Another possibility is that a "true" steady-state was not achieved in our NO oxidation experiments even after performing the experiments for a few hours. As described in the next section, transient NO oxidation experiments showed that a steady-state is not achieved even after 14 h. So, the "apparent" steady-state used for the calculation of activation energies might give erroneous results. The above activation energy comparisons notwithstanding, it should be mentioned that the rate of NO oxidation depends on the Pt particle size [2,11,20]. Mulla et al. [9] argued that in the absence of NO_2, the measured rate is inversely dependent on the conversion, even at low conversions. These points make comparisons of kinetic parameters between various literature studies more difficult.

4.1.2. Transient experiments

While performing the steady-state NO oxidation experiments, the time taken to achieve a steady-state for temperatures less than 185 °C was about 30–60 min, as discussed before in the experimental section. At a slightly higher temperature, the reactor system was left overnight at 202.5 °C to achieve steady-state. From Fig. 3, it is observed that the steady-state data point at 202.5 °C does not fall along the anticipated extrapolation from the lower temperature data points. Indeed, at temperatures higher than 180.8 °C, the local slope of the conversion curve exhibits a slight decrease from the slope at lower temperatures (150–180.8 °C). An estimate of the characteristic reaction time showed that at temperatures greater than 180.8 °C, the transverse diffusion time is of the order of the characteristic reaction time. Also, the Weisz modulus is of the order of 1. Thus, one reason for the slope change could be mass transfer limitations to the surface and/or diffusional limitations in the washcoat. However, even though not shown in the current work, modeling studies showed that diffusional limitations alone are not responsible for the observed decrease in the NO oxidation rates. Moreover, it is unlikely that diffusional processes would cause the protracted approach to steady-state.

Since the steady-state data point at 202.5 °C was obtained by running the experiment for 14 h, deactivation of the catalyst could be another factor governing the observed slope change. Fig. 5 shows the transient NO_2 concentration profile observed during the overnight NO oxidation experiment. The initial increase in NO_2 concentration is due to an increase in catalyst temperature since it took approximately 6 minutes for the catalyst temperature to reach a constant value of 202.5 °C. Even though the catalyst temperature was constant throughout the rest of the experiment, the NO_2 concentration was observed to decrease monotonically with time, suggesting a decrease in oxidation activity. Fig. 5 also shows the transient variation of concentration of total N exiting the reactor. The total N effluent concentration was evaluated by measuring the concentration of N-containing gaseous species, except N_2, which could not be measured in the FT-IR and would not be expected as a product under the reaction conditions. The total N outlet concentration was essentially constant during the entire experiment. At the start of this experiment, NO_x was present on the catalyst from the previous experiment at 180.8 °C. Hence, the change in temperature from 180.8 °C to 202.5 °C did not result in observable decrease in the total N outlet concentration, suggesting that there is negligible accumulation of N species on the catalyst. Thus, the observed decrease in NO oxidation rate is not caused by NO_x storage, but is due to the loss in catalyst activity. Similar results were observed by Olsson and Fridell [6] over a Pt/Al_2O_3 catalyst when the feed gas contained a mixture of NO and O_2.

In order to investigate the transient response of the NO oxidation activity at lower temperatures, an experiment with an inlet NO concentration of 634 ppm and excess O_2 (5%) was performed on a pre-reduced catalyst at a temperature of 106 °C. The resulting NO_2 concentration profile was monitored, and is shown in Fig. 6. It is observed that the outlet NO_2 concentration decreases with time, although the rate of decrease is smaller than that observed during the higher temperature experiment shown in Fig. 5. Even though the decrease in NO_2 concentration is small in absolute units, the percentage change between the maximum NO_2 concentration and the concentration after 15 h is 22%. Hence, the results in Figs. 5 and 6 show that there is a continuous decrease in the NO oxidation rates with time at high as well as low temperatures. This poses a challenge in achieving a steady-state and in determining the steady-state kinetics for the oxidation reaction.

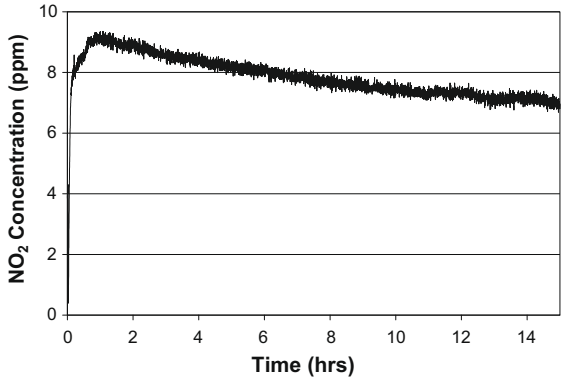

Fig. 6. Transient NO_2 concentration profile for a feed consisting of 634 ppm NO and 5% O_2 over $Pt/BaO/Al_2O_3$ catalyst (catalyst temperature = 106 °C).

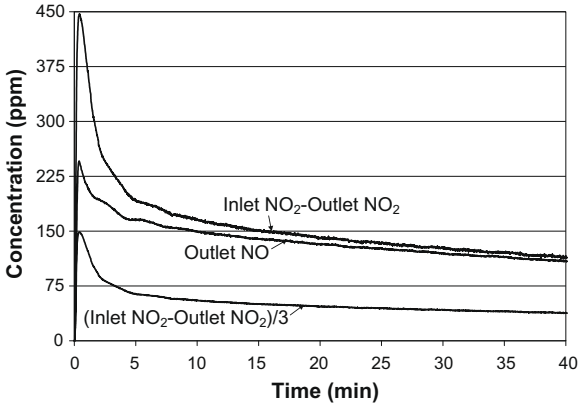

Fig. 8. Comparison of exit NO concentrations and NO_2 consumed for a feed of NO_2 over $Pt/BaO/Al_2O_3$ catalyst (inlet NO_2 = 484 ppm, catalyst temperature = 313 °C).

As mentioned above, NO_2 storage was found to play an insignificant role in the observed decrease in oxidation activity. To study the role of NO_2 either as a source of NO or as an oxidant, experiments were performed in which the feed gas consisted of NO_2 at various concentration levels and temperatures. It has been reported in the literature that NO_2 storage on Pt/BaO catalysts occurs according to a disproportionation reaction, in which 1 mole of NO is produced for every 2 moles of NO_2 stored [21–23]. This is equivalent to the consumption of 3 moles of NO_2 for every mole of NO produced on either the BaO or exposed Al_2O_3 support:

$$3NO_2 + BaO \rightarrow Ba(NO_3)_2 + NO$$
$$9NO_2 + Al_2O_3 \rightarrow 2Al(NO_3)_3 + 3NO$$

A comparison of the NO outlet concentration and one-third of the difference between the inlet and outlet NO_2 concentrations is shown in Fig. 7, for an inlet NO_2 concentration of 555 ppm and a catalyst temperature of 100 °C. The two curves essentially overlap, thus validating the disproportionation reactions. This result also suggests that for transient modeling studies of NO oxidation, the role of NO_2 storage in generating NO cannot be neglected even at low temperatures. On the other hand, incorporating NO_2 storage in the model is not required for steady-state NO oxidation modeling. A comparison of the outlet NO concentration and difference between the inlet and outlet NO_2 concentrations at a higher catalyst temperature (313 °C) is shown in Fig. 8 for an inlet NO_2 feed concentration of 484 ppm. It is observed that the moles of NO produced are almost equal to the moles of NO_2 consumed at longer times, resulting in a ratio of approximately 1 between them. This is in contrast to the ratio of 0.33 for the experiment at 100 °C. This suggests that at higher temperatures, NO is produced by NO_2 decomposition in addition to NO_2 storage, since the decomposition reaction has a stoichiometry of 1 between NO consumed and NO_2 produced. Kabin et al. [23] performed experiments on $Pt/BaO/Al_2O_3$ catalysts having varied Pt loadings to study the relative contribution of NO_2 storage and decomposition in the formation of NO. They reported that the ratio of moles of NO produced and NO_2 consumed achieved a value close to 0.33 for the catalyst with no Pt at 340 °C. This ratio increased with the increase in Pt loading and approached a value of unity for the catalyst with the highest Pt loading, which is indicative of NO_2 decomposition. Fig. 7 shows that after flowing NO_2 over the catalyst for 40 min, less than 10 ppm NO is observed in the outlet at 100 °C. This is because the only mechanism of NO formation at low temperatures is NO_2 storage, and the sample gets saturated with stored NO_2 after some time because of a finite NO_x storage capacity. However, more than 100 ppm NO is observed at 313 °C after 40 min, as seen in Fig. 8, since NO is formed mainly by decomposition at a high temperature. In summary, at low temperatures, NO is formed by NO_2 storage on a $Pt/BaO/Al_2O_3$ catalyst, whereas NO_2 decomposition is the primary route for NO formation at higher temperatures.

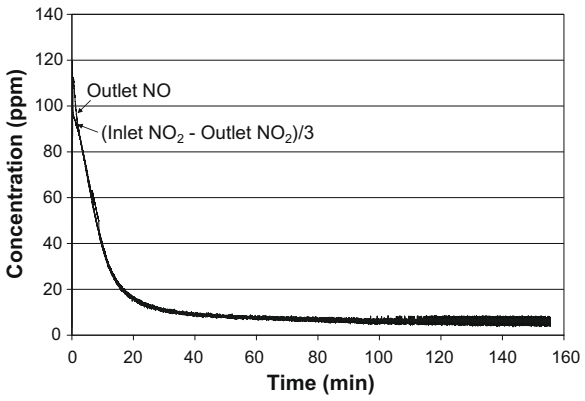

Fig. 7. Comparison of exit NO concentrations and NO_2 consumed for a feed of NO_2 over $Pt/BaO/Al_2O_3$ catalyst (inlet NO_2 = 555 ppm, catalyst temperature = 100 °C).

4.2. Pt/Al_2O_3

The concurrence of NO oxidation and NO_x storage poses a challenge for the study of NO oxidation in isolation. In order to reduce the NO_2 storage effects and to study the role of NO_2 during NO oxidation, additional experiments were performed on a Pt/Al_2O_3 catalyst (sample A3). (Remark: Storage on the Al_2O_3 support is about half of the total storage on BaO/Al_2O_3 for temperatures above 250 °C [24].) Steady-state experiments, similar to those on $Pt/BaO/Al_2O_3$ (sample B4), were carried out for inlet NO and O_2 concentrations of 482 ppm and 5%, respectively. The highest turnover frequency (TOF) was estimated to be 0.1 mol NO_2/mol exposed Pt s^{-1} at 256 °C. Mulla et al. [11] reported a TOF of 3.5×10^{-3} mol NO/mol Pt s at a temperature of 300 °C when the feed consisted of 300 ppm NO, 170 ppm NO_2, and 10% O_2. As will be shown later, in the presence of 328 ppm NO and 92 ppm NO_2, we calculated the TOF at 189 °C to be equal to 5.77×10^{-3} mol NO_2/mol exposed Pt s^{-1}. In contrast, Smeltz et al. [25] reported a very high TOF of 0.34 s^{-1} at 300 °C on Pt(1 1 1) for a feed consisting of 73 ppm NO, 27 ppm NO_2, and 5% O_2. The difference between the turnover rates reported in the literature could be due to the different concentrations of NO_2 used, which can inhibit the NO oxidation reaction, as discussed later. The Pt particle size has been reported to affect the NO oxidation rates [2,11,20], with the large Pt particle size resulting in high turnover rates. The higher TOF reported by Smeltz

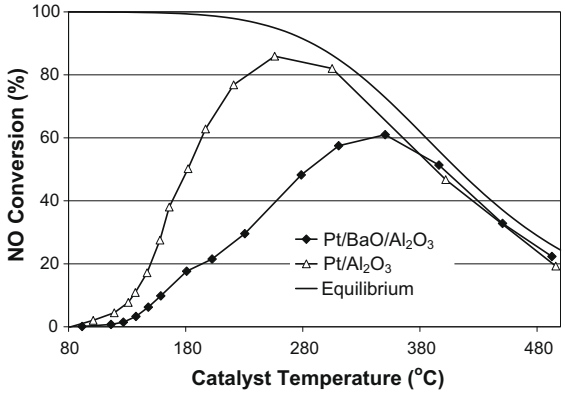

Fig. 9. Comparison of steady-state NO conversions for Pt/Al_2O_3 (A3) and $Pt/BaO/Al_2O_3$ (B4) catalysts (inlet NO = 528 ppm for $Pt/BaO/Al_2O_3$ and 482 ppm for Pt/Al_2O_3; inlet O_2 = 5% for both cases).

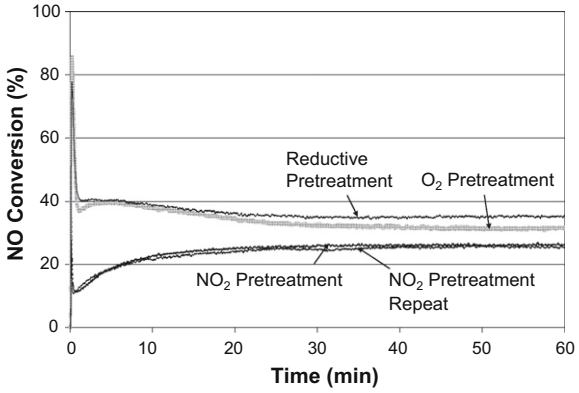

Fig. 10. Comparison of transient NO conversion for various pretreatments on Pt/Al_2O_3 catalyst (inlet NO = 500 ppm, O_2 = 5%; catalyst temperature = 198 °C).

et al. [25] was attributed to the closer-packed Pt atoms on the (1 1 1) plane which may be more resistant to oxidation.

The activation energy of the NO oxidation reaction was estimated to be 75.9 kJ/mol for the Pt/Al_2O_3 catalyst compared to 81.8 kJ/mol for the $Pt/BaO/Al_2O_3$ catalyst. A comparison of the NO conversions for catalysts A3 and B4 is shown in Fig. 9. Since the dispersion, loading, and volume of the catalysts used were not the same for the two cases, a direct comparison of the two curves is difficult. (The moles of Pt exposed were estimated for catalysts A3 and B4 to be 8.8×10^{-6} and 2.1×10^{-5}, respectively.) Similar to the $Pt/BaO/Al_2O_3$ catalyst, the slope of the conversion vs. temperature curve for the Pt/Al_2O_3 catalyst is lower for temperatures greater than 180 °C as compared to temperatures less than 180 °C, although the magnitude of change in slope is smaller than that for the $Pt/BaO/Al_2O_3$ catalyst. At higher temperatures (>375 °C), NO conversions are similar for both the catalysts since the reaction is thermodynamically limited. On the other hand, at lower temperatures (<350 °C), the NO conversion for Pt/Al_2O_3 is higher than for $Pt/BaO/Al_2O_3$, even though the total exposed Pt was higher for the latter. This is in agreement with the results reported in the literature [3,6,8].

One reason for the lower activity of the $Pt/BaO/Al_2O_3$ catalyst could be the storage of NO_x on the catalyst, which results in the formation of bulky nitrites/nitrates. This could result in the blocking of Pt sites by the BaO storage phase, thus rendering some of the Pt inaccessible to NO_x in the gas phase. Olsson and Fridell [6] performed XPS measurements after exposing Pt/Al_2O_3 and $Pt/BaO/Al_2O_3$ catalysts to NO_2 and observed a higher concentration of platinum oxides on the $Pt/BaO/Al_2O_3$ catalyst in comparison to the Pt/Al_2O_3 catalyst. This observation could explain the reduced activity of $Pt/BaO/Al_2O_3$ catalyst as compared to that of a Pt/Al_2O_3 catalyst. This could also explain the greater change in the slope of the conversion vs. temperature curve for the $Pt/BaO/Al_2O_3$ catalyst compared to that for the Pt/Al_2O_3 catalyst. A theory on the effect of support on the formation of Pt oxides has been given by Yoshida et al. [26]. They proposed that if Pt is present on an acidic support (which is electrophilic), there is a lower electron density on Pt due to the donation of electrons to the support. Since the formation of oxides involves the transfer of electrons from Pt to oxygen, an acidic support (e.g. Al_2O_3) would result in a lower amount of oxide formation as compared to an alkaline support (e.g. BaO). It needs to be mentioned again that, as in the case of catalyst B4, the steady-state rates reported here for intermediate temperatures (180–250 °C) may not be the "true" steady-state values, since the NO oxidation activity decreased with time. At low temperatures, the decrease in activity was nominal and could be neglected, whereas at higher temperatures (>250 °C), the reaction rates were close to equilibrium due to which a steady-state was achieved quickly.

Since the attainment of a steady-state took a very long time and the actual operation of a NO_x trap involves transient processes, we chose to perform transient rather than "steady-state" experiments with NO and NO_2 hereafter. To investigate the cause of the transient decrease in NO oxidation rates, pretreatment experiments were accomplished by flowing O_2 or NO_2 over the catalyst before performing the NO oxidation experiment, the details of which are described in the experimental section. Fig. 10 shows the transient NO conversion profiles after various catalyst pretreatments. The inlet gas was at a temperature of 192 °C and was composed of 500 ppm NO and 5% O_2. 'NO_2 Pretreatment Repeat' in the figure refers to the results of the repeat experiment for the case of NO_2 pretreatment. The results of the repeat NO_2 pretreatment experiment match very well with the original results; this affirms the reproducibility of the experimental results.

It is observed from Fig. 10 that after 60 min, the NO conversion was the highest for the reductive pretreatment, whereas the NO conversion was the lowest when the catalyst was pretreated with NO_2. This indicates that NO_2 inhibits NO oxidation, either as adsorbed NO_2 or through the oxidation of the Pt catalyst. It was shown earlier for the $Pt/BaO/Al_2O_3$ catalyst that NO_2 storage on the catalyst played an insignificant role in suppressing the NO oxidation rates. Since the Pt/Al_2O_3 catalyst was used for the pretreatment experiments, the storage of NO_2 on the catalyst would be even less, at least at moderate to high temperatures when adsorption on alumina is negligible. Hence, the role of stored NO_2 in decreasing the NO oxidation reaction rates can be neglected.

The lowest NO conversion for the case of NO_2 pretreatment can be explained by the highly oxidizing nature of NO_2, which reduces the catalytic activity. In independent studies, Segner et al. [27] and Parker and Koel [28] showed that NO_2 can be an effective source of atomic oxygen because of its high sticking coefficient. The chemisorbed oxygen, which is the most abundant species, prevents adsorption of other species, thus inhibiting the reaction. The XPS results of Olsson and Fridell [6] suggest the formation of platinum oxide on exposing the catalyst to NO_2, which has a lower activity for NO oxidation as compared to that for the reduced form of Pt. This helps to explain the results in Fig. 10, which show a lower NO conversion after NO_2 pretreatment as compared to the reductive pretreatment. Olsson and Fridell [6] also showed that exposing the Pt catalyst to O_2 results in the formation of Pt oxides. This result is consistent with the lower NO conversion found after O_2 pretreatment as compared to the reductive pretreatment. We found that O_2 pretreatment results in a higher NO conversion as compared to NO_2 pretreatment, even though O_2 pretreatment was

done with a much higher concentration of 5% as compared to the pretreatment with only 524 ppm NO_2. This is likely a result of the highly oxidizing nature of NO_2 as compared to O_2. Getman et al. [29] observed that similar pressures of O_2 and NO_2 resulted in higher O coverages on Pt(1 1 1) by NO_2 than O_2, which was attributed to the faster kinetics of the NO_2 dissociation reaction as compared to that of O_2 dissociation. Parker and Koel [28] used NO_2 at temperatures above 400 K to generate oxygen coverages of 0.75 monolayers on Pt(1 1 1), whereas only 0.25 monolayers of atomic oxygen have been reported to adsorb on Pt(1 1 1) using gaseous O_2 [30].

In analyzing the transient NO conversion profiles in Fig. 10, it should be noted that the transient NO conversions approach 90% during the first minute. The outlet total N concentration was plotted as a function of time (not shown here) and it was less than the inlet N concentration. Thus, the initial high NO conversion can be attributed to the storage of NO_x on Pt/Al_2O_3. This is consistent with the previous studies which reported NO_2 sorption on Al_2O_3 [24,31]. The small minimum observed at around 1 min for the case of O_2 pretreatment may be due to the non-attainment of a steady temperature at short times. The transient NO conversion profiles show that NO conversion decreases with time for the reductive and O_2 pretreatments. This is probably a result of the NO_2 formed during the reaction, which oxidizes the Pt catalyst. Interestingly, however, the NO conversion increases with time for the case of NO_2 pretreatment, but is less than the conversion level achieved with the reductive and the oxidative pretreatments for all times. The transient increase can be explained by the reaction of NO with surface oxygen deposited during NO_2 pretreatment. However, after 60 min, NO conversion after NO_2 pretreatment is less than that after reductive pretreatment and the difference indicates the formation of irreversible Pt oxides. For the case of O_2 pretreatment, the difference in conversion is smaller, indicating that the amount of Pt oxide formation is lower than in the case of NO_2 pretreatment.

The findings in Fig. 10 pose a compelling case for the formation of chemisorbed oxygen/Pt oxides, which are responsible for the transient decrease in NO oxidation rates. Whereas chemisorbed oxygen can react with NO resulting in the restoration of the catalyst activity, the formation of Pt oxides results in the loss of activity, which is not regained during the oxidation reaction. The catalyst can however be regenerated by reduction with H_2, which can be seen by the reproducibility of the transient NO conversion curves after NO_2 pretreatment. However, it is observed that there is a significant difference in steady-state NO conversion at 198 °C (Fig. 9) and the NO conversion after reductive pretreatment at the same temperature (Fig. 10). This could be due to the irreversible aging of the catalyst over a prolonged period of time. O_2 can also result in the reduction of the activity, but the contribution of O_2 in oxidizing the catalyst is small as compared to that of NO_2. The non-attainment of a steady-state while performing the NO oxidation experiments on $Pt/BaO/Al_2O_3$ and Pt/Al_2O_3 is also due to the slow oxidation of the catalysts by NO_2 generated during the reaction and partly by O_2 fed to the reactor.

In order to provide further evidence on the role of NO_2 in reducing the NO oxidation reaction rate, transient NO oxidation experiments with 328 ppm NO and 5% O_2 were performed for various inlet NO_2 concentrations, the results of which are shown in Fig. 11. The catalyst temperature used was 189 °C to minimize the extent of the NO_2 decomposition reaction. The experiment with 92 ppm NO_2 was done first, followed by the 0 ppm NO_2 experiment; the experiment with 208 ppm NO_2 was done in the end to avoid systematic errors. It is observed that the transient as well as steady-state NO conversions decrease with an increase in inlet NO_2 concentration, further illustrating the inhibition by NO_2. As is mentioned for Fig. 10, high instantaneous NO conversions approaching 95% are due to NO_x storage on the catalyst. The marginal increase in NO conversion for the case of 208 ppm NO_2 between 10 and 20 min of the experiment could be a result of the consumption of NO by chemisorbed O, as mentioned earlier in reference to the NO_2 pretreatment experiment.

Since it is now established that NO_2 inhibits the NO oxidation reaction, further experiments were performed to study the inhibiting effect of NO_2 on the NO_2 decomposition reaction on Pt/Al_2O_3. The switch to Pt/Al_2O_3 catalyst from $Pt/BaO/Al_2O_3$ for the transient experiments was made to minimize the NO_x storage effects in studying NO oxidation and decomposition systems. However, the exit NO_x concentration took a few minutes to achieve a value equal to the inlet NO_x concentration for all the experiments, indicating that NO_x storage, even though lower than $Pt/BaO/Al_2O_3$, occurs on Pt/Al_2O_3 as well. Fig. 12 shows the effect of catalyst temperature on the transient exit NO concentration profiles for a feed consisting of 535 ppm NO_2. It is observed that after the initial increase, the exit NO conversion decreases with time for all temperatures. An analysis of the exit total N concentration and the integral ratio of the moles of NO produced to the moles of NO_2 consumed reveals that NO_2 storage and decomposition occur on Pt/Al_2O_3 at low temperatures (190 °C and 287 °C), whereas at 369 °C, the main route for NO formation is NO_2 decomposition. The transient decrease in exit NO concentration for low temperatures is explained by the limited NO_x storage capacity. However, at 369 °C, storage on Pt/Al_2O_3 is negligible and thus the observed decrease in activity is explained by the role of NO_2 in oxidizing the catalyst. The NO_2 inhibition effect could also contribute to the observed transient

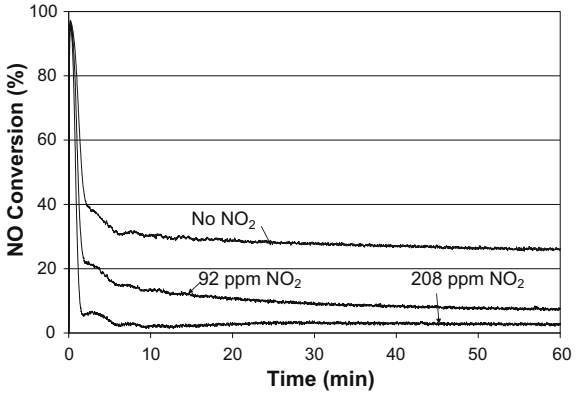

Fig. 11. Comparison of transient NO conversion for various inlet NO_2 concentrations (inlet NO = 328 ppm, O_2 = 5%; catalyst temperature = 189 °C; Pt/Al_2O_3 catalyst).

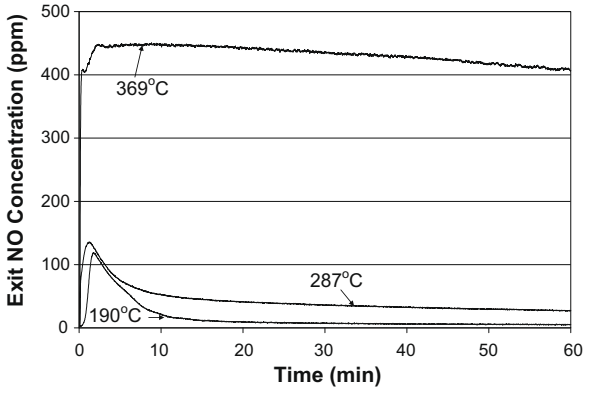

Fig. 12. Comparison of transient exit NO concentrations for various catalyst temperatures (inlet NO_2 = 535 ppm; Pt/Al_2O_3 catalyst).

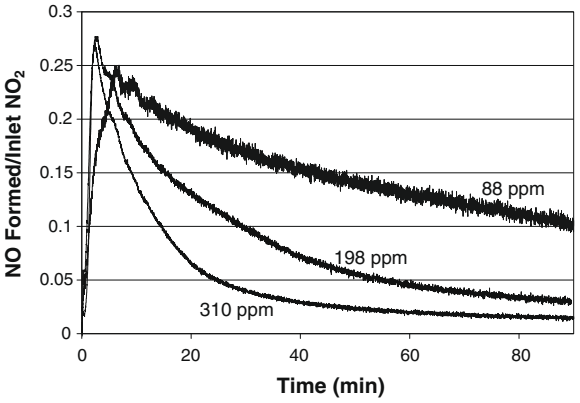

Fig. 13. Transient variation of the ratio of outlet NO concentration to inlet NO_2 concentration for various inlet NO_2 concentrations (catalyst temperature = 190 °C; Pt/Al_2O_3 catalyst).

activity decrease at low temperatures. However, the individual contribution of NO_2 storage and inhibition effects could not be quantified.

To study the effect of inlet NO_2 concentration on the NO_2 decomposition reaction, experiments were performed on Pt/Al_2O_3 catalyst at a relatively low temperature (190 °C), with the inlet NO_2 concentration varying between 88 ppm and 310 ppm. The ratio of outlet NO concentration to the inlet NO_2 concentration is shown as a function of time in Fig. 13. We refer to this ratio as the 'relative NO concentration' in the discussion hereafter. It is observed that the relative NO concentration goes through a maximum with time for each inlet NO_2 concentration; this is attributed to NO_x storage. For inlet NO_2 concentrations of 198 ppm and 310 ppm, the transient ratio profiles before the attainment of the maximum almost overlap with each other. However, for the lowest inlet NO_2 concentration of 88 ppm, the ratio is somewhat lower, which is due to the higher relative amounts of NO_x stored (moles of NO_x stored/inlet moles of NO_2). It is also observed in Fig. 13 that the time at which the NO concentration achieves a maximum decreases with an increase in inlet NO_2 concentration. Also, the slope of the decrease in the relative NO concentration is the highest for 310 ppm NO_2 and lowest for 88 ppm NO_2. Finally, it is observed that after 90 min, the relative outlet NO concentration is the highest for the lowest inlet NO_2 concentration, and decreases with an increase in the inlet NO_2 concentration. These trends can be explained by the fact that a higher NO_2 concentration results in a higher concentration of chemisorbed oxygen/Pt oxides, which leads to an earlier and faster reduction in the activity of the catalyst. Although not explicitly shown here, the outlet NO concentration is found to decrease with an increase in the inlet NO_2 concentration. This can again be explained by a higher reduction in the catalytic activity for a higher NO_2 concentration. This result also explains the negligible catalyst poisoning for the low temperature NO oxidation experiments (Fig. 3). In this regime, the low NO conversion results in a rather low concentration of NO_2, thus explaining the negligible deactivation.

4.3. Modeling results

Hauptmann et al. [12] performed a comparative study between literature global kinetic models and found that all the models showed deviations between the calculated and experimentally obtained NO conversions. They reported that Marques et al. [7] did not consider the NO_2 decomposition reaction in their rate expression, which resulted in a prediction of NO conversions greater than the equilibrium values. Hauptmann et al. [12] also used the global kinetic models proposed by Mulla et al. [9] and Olsson et al. [32] to predict the experimental steady-state NO conversions at various temperatures. However, these models were not able to predict the data. This is probably because Olsson et al. [32] did not consider the inhibitory effect of NO_2 on the NO oxidation reaction. As discussed later, Mulla et al. [9] neglected the surface coverage of NO on Pt while deriving a global rate expression, which is not a valid assumption at low temperatures. Moreover, Olsson et al. [13] found the reaction $NO + O - S \rightarrow NO_2 - S$ to be the rate-determining step for the NO oxidation. This is in contrast to the studies by Mulla et al. [9] who assumed O_2 adsorption on the catalyst surface as the rate-determining step to derive a global rate expression, which was consistent with their experimental observations.

To determine the rate-determining step of the NO oxidation reaction and to understand the surface chemistry, we performed a steady-state analysis of a microkinetic reaction scheme taken from the literature [33]. It consists of the reversible adsorption and desorption of NO, O_2, and NO_2 combined with the reversible surface reaction of the adsorbed NO and O to form adsorbed NO_2 and is given as follows:

Step 1a. $NO + Pt \leftrightarrow NO - Pt$

Step 2a. $O_2 + 2Pt \leftrightarrow 2O - Pt$

Step 3a. $NO - Pt + O - Pt \leftrightarrow NO_2 - Pt + Pt$

Step 4a. $NO_2 + Pt \leftrightarrow NO_2 - Pt$

Pt in steps (1a)–(4a) refers to a vacant Pt site. Assuming mass action kinetics, the rates of steps (1a)–(4a) are given by

$$R_{v1} = k_{f1} X_{NO,s} \theta_v - k_{b1} \theta_{NO} \quad (4.5)$$

$$R_{v2} = k_{f2} X_{O_2,s} \theta_v^2 - k_{b2} \theta_O^2 \quad (4.6)$$

$$R_{v3} = k_{f3} \theta_{NO} \theta_O - k_{b3} \theta_{NO_2} \theta_v \quad (4.7)$$

$$R_{v4} = k_{f4} X_{NO_2,s} \theta_v - k_{b4} \theta_{NO_2} \quad (4.8)$$

k_{fi} and k_{bi} in Eqs. (4.5)–(4.8) refer to the forward and reverse rate constants of step i, respectively, whereas θ_j and θ_v refer to the fractional surface coverage of species j and the vacant site coverage, respectively. The forward and reverse rate constants for step i are defined as

$$k_{fi} = A_{fi} e^{-E_{fi}/RT_s} \quad (4.9)$$

$$k_{bi} = A_{bi} e^{-E_{bi}/RT_s} \quad (4.10)$$

where A_{fi} and A_{bi} are the pre-exponential factors and E_{fi} and E_{bi} are the activation energies of step i, respectively. The values of the pre-exponential factors and activation energies used in the simulations were taken from Xu et al. [33] and are given in Table 7. These values satisfy the enthalpic as well as the entropic constraints and were originally reported by Olsson et al. [3] from O_2 TPD and NO oxidation experiments on a Pt/Al_2O_3 catalyst.

The short monolith model given in Table 4 combined with Eqs. (4.5)–(4.8) is used to predict the steady-state NO conversion and coverages of various adsorbed species as a function of inlet tem-

Table 7
Values of microkinetic reaction parameters used in the simulations.

Parameter	Numerical value (mol/m^3 washcoat s)	Parameter	Numerical value (kJ/mol)
A_{f1}	7.5×10^9	E_{f1}	0
A_{b1}	5.7×10^{17}	E_{b1}	114.5
A_{f2}	4.7×10^8	E_{f2}	30.4
A_{b2}	5.8×10^{16}	E_{b2}	209.4
A_{f3}	4.5×10^{14}	E_{f3}	101.3
A_{b3}	2.5×10^{14}	E_{b3}	52.5
A_{f4}	8×10^9	E_{f4}	0
A_{b4}	5.7×10^{17}	E_{b4}	97.9

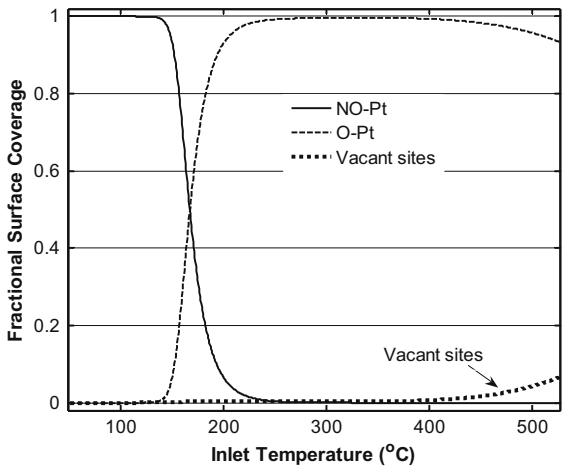

Fig. 14. Variation of fractional surface coverage with inlet temperature (inlet NO = 328 ppm, O_2 = 5%, Pt/Al_2O_3 catalyst).

perature for a feed consisting of 328 ppm NO and 5% O_2. As expected, the model predicts that with an increase in inlet temperature, the NO conversion increases in the kinetic regime and decreases in the equilibrium limited regime. The variation of fractional surface coverages of various adsorbed species with an increase in inlet temperature is shown in Fig. 14. It is observed that adsorbed NO predominantly covers the catalyst surface at low temperatures (<150 °C), which is due to its high sticking coefficient on Pt. As the temperature is increased, the surface becomes predominantly covered with O until, at a very high temperature (~400 °C), adsorbed O starts desorbing which results in an increase in the vacant site coverage. The coverage of NO_2 is found to be small as compared to the other adsorbed surface species (maximum NO_2 coverage is 2.3×10^{-4} at 171 °C) and hence is not shown in the figure.

A parametric sensitivity analysis of the various pre-exponential factors was done to determine the rate-determining step. Both the forward and the reverse pre-exponential factors were multiplied by the same factor while keeping all other parameters fixed in order to keep the equilibrium constant fixed and hence to ensure thermodynamic consistency. On performing the sensitivity analysis on all the four reaction steps, it was found that changing the rates of steps (1a), (3a), and (4a) resulted in a negligible change in the predicted NO conversion. However, a change in the pre-exponential factor for step 2a, i.e. O_2 adsorption/desorption, resulted in a significant change in the predicted NO conversion, hence suggesting O_2 adsorption/desorption to be the rate-determining step. Parametric sensitivity analysis and estimation of surface coverages was also performed for a feed consisting of 535 ppm NO_2 for various temperatures. It was found that O_2 desorption from the surface was rate-determining and the predominant surface species was adsorbed O over a wide range of temperatures. Getman et al. [29] showed by DFT studies that O_2 desorption remains a highly activated process even at high O coverages. Hence, one reason for the transient decrease in NO concentration while feeding NO_2 at 190 °C (Fig. 13) could be the accumulation of adsorbed O on the surface, which does not desorb at these low temperatures (Fig. 14).

Based on the microkinetic analysis, we develop here a global model assuming O_2 adsorption as the rate-limiting step. An explicit global rate model is more appealing than a microkinetic model because of its much simpler application in reactor modeling. However, a global model requires the existence of a single rate-determining step over the operating range of interest. To investigate this issue, consider the following set of steps:

Step 1b. $NO + Pt \leftrightarrow NO - Pt$

Step 2b. $O_2 + Pt \leftrightarrow O_2 - Pt$

Step 3b. $NO - Pt + O - Pt \leftrightarrow NO_2 - Pt + Pt$

Step 4b. $NO_2 + Pt \leftrightarrow NO_2 - Pt$

Step 5b. $O_2 - Pt + Pt \leftrightarrow 2O - Pt$

O_2 adsorption is assumed to proceed through a molecular precursor (step 2b), followed by the dissociation of the precursor to atomic oxygen (step 5b). This is because it has been shown experimentally and theoretically that oxygen dissociation on Pt surface proceeds via a precursor-mediated reaction path [34–36].

The rates of steps (1b), (3b), and (4b) are given by Eqs. (4.5), (4.7), and (4.8), respectively, whereas the rates of steps (2b) and (5b) are given as

$$R_{v2} = k_{f2} X_{O_2,s} \theta_v - k_{b2} \theta_{O_2} \tag{4.11}$$

$$R_{v5} = k_{f5} \theta_{O_2} \theta_v - k_{b5} \theta_O^2 \tag{4.12}$$

The microkinetic parametric sensitivity analysis showed that steps (1b), (3b), and (4b) are fast in comparison to the adsorption/desorption of O_2 and hence are assumed to be in equilibrium. Also, the dissociation of adsorbed molecular oxygen (step 5b) is assumed to be fast and in equilibrium. Zambelli et al. [36] observed that the interaction between chemisorbed O atoms and precursor O_2 molecules results in an increase in the dissociation probability of the precursor molecules. This justifies our assumption of fast dissociation of molecularly adsorbed O_2, since it is shown by microkinetic studies that chemisorbed O is the predominant species on the surface for a wide temperature range (Fig. 14). On making these assumptions, we obtain the surface coverages of the various species as

$$\theta_{NO} = K_1 X_{NO,s} \theta_v \tag{4.13}$$

$$\theta_{NO_2} = K_4 X_{NO_2,s} \theta_v \tag{4.14}$$

$$\theta_O = \frac{1}{K_3} \frac{K_4 X_{NO_2,s}}{K_1 X_{NO,s}} \theta_v \tag{4.15}$$

$$\theta_{O_2} = \frac{1}{K_5} \left(\frac{1}{K_3} \frac{K_4 X_{NO_2,s}}{K_1 X_{NO,s}} \right)^2 \theta_v \tag{4.16}$$

K_i in Eqs. (4.13)–(4.16) represents the equilibrium constant of step i. An overall site balance gives the following expression for the vacant site coverage:

$$\theta_v = \frac{1}{1 + K_1 X_{NO,s} + K_4 X_{NO_2,s} + \frac{1}{K_3} \frac{K_4 X_{NO_2,s}}{K_1 X_{NO,s}} + \frac{1}{K_5} \left(\frac{1}{K_3} \frac{K_4 X_{NO_2,s}}{K_1 X_{NO,s}} \right)^2} \tag{4.17}$$

Assuming molecular O_2 adsorption to be the rate-determining step, the rate of NO oxidation is given as

$$R_{v,NO\_ox} = k_{f2} X_{O_2,s} \theta_v - k_{b2} \theta_{O_2}$$
$$= k_{f2} X_{O_2,s} \left[1 - \frac{1}{X_{O_2,s} K_2 K_5} \left(\frac{1}{K_3} \frac{K_4 X_{NO_2,s}}{K_1 X_{NO,s}} \right)^2 \right] \theta_v$$

where θ_v is given by Eq. (4.17). From the microkinetic analysis, it was shown that the surface coverage of adsorbed NO_2 (Eq. (4.14)) is much smaller than the coverages of O and NO in the desired temperature range (100–450 °C), and hence can be neglected. A similar assumption is made regarding the coverage of the molecular oxygen species (Eq. (4.16)) based on the fact that most sites are occupied by either O or NO. In addition, the adsorption parameters for NO and O_2 (Table 7) predict lower adsorption rates of O_2 compared to those of NO even for a feed gas containing a much higher concentration of O_2. This lends credence to our assumption of O_2 adsorption as the rate-determining step. These

assumptions lead to a simplified expression for the vacant site coverage as

$$\theta_v = \frac{1}{K_1 X_{NO,s} + \frac{1}{K_3}\frac{K_4 X_{NO_2,s}}{K_1 X_{NO,s}}} \tag{4.18}$$

Using Eq. (4.18), the rate of NO oxidation simplifies to

$$R_{v,NO\_ox} = k_{f2} X_{O_2,s}\left[1 - \frac{1}{X_{O_2,s} K_2 K_5}\left(\frac{1}{K_3}\frac{K_4 X_{NO_2,s}}{K_1 X_{NO,s}}\right)^2\right]\frac{1}{K_1 X_{NO,s} + \frac{1}{K_3}\frac{K_4 X_{NO_2,s}}{K_1 X_{NO,s}}} \tag{4.19}$$

$$= k_{f2} X_{O_2,s}\left[1 - \left(\frac{X_{NO_2,s}}{K_{eq}\sqrt{X_{O_2,s}} X_{NO,s}}\right)^2\right]\frac{1}{K_1 X_{NO,s} + \frac{1}{K_3}\frac{K_4 X_{NO_2,s}}{K_1 X_{NO,s}}} \tag{4.20}$$

K_{eq} in Eq. (4.20) is the equilibrium constant of the overall NO oxidation reaction and is given by

$$K_{eq} = \frac{K_1 K_3}{K_4}\sqrt{K_2 K_5} \tag{4.21}$$

The global model given by Eq. (4.20) predicts that the rate of NO oxidation is inhibited by NO_2, which is consistent with our experimental results (Fig. 11) and previous reports in the literature [9,11]. In order to check the validity of our assumption of molecular O_2 adsorption as the rate-determining step, we derived a global rate expression for NO oxidation assuming dissociation of adsorbed molecular O_2 (step 5b) as the rate-determining step. However, it predicted the reaction to be '+2' order with respect to NO and '−2' order with respect to NO_2, which is in contrast to the experimental observations [9,11]. Even though our microkinetic analysis showed O_2 adsorption as the rate-determining step, we derived global rate expressions assuming various rate-determining steps to check if there could be multiple rate expressions which fit the experimental data. But, none of the rate expressions predicted the correct reaction orders with respect to NO, O_2, and NO_2. For example, the assumption of NO adsorption or reaction between adsorbed NO and O as the rate-determining step predicted that the reaction would be negative order with respect to O_2. Furthermore, the assumption of NO_2 desorption as the rate-determining step predicted a zero-order dependence of NO_2 on the reaction rate, which is inconsistent with the reported experimental data [9,11].

Eq. (4.20) is used to predict the steady-state NO oxidation experiment results on the Pt/Al_2O_3 catalyst. Several of the kinetic parameters are used from the microkinetic model (Table 7). However, some of the parameters were modified and are given in Table 8. O_2 adsorption is assumed to be non-activated in accordance with the literature [34]. In order to maintain thermodynamic consistency, the activation energies of NO desorption (step 1b) and the dissociation of NO_2–Pt (step 3b) were increased. Also, the pre-exponential factor for NO desorption was reduced to account for the reduced activation energy. It was verified that the kinetic parameters in Table 8 satisfy the thermodynamic and entropic constraints. Using these values, the model predicts high surface coverages of adsorbed NO and O at low and high temperatures, respectively. Also, a low vacant site coverage is predicted for the entire temperature range. A comparison of experimental data and model predictions is given in Fig. 15. The model predictions are in excellent agreement with the experiment results. Mulla et al. [9] also derived a global rate expression for NO oxidation by assuming O_2 adsorption as the rate-limiting step. They assumed that O–Pt is the predominant surface species over the entire temperature range. However, we showed from our microkinetic analysis that the coverage of NO cannot be neglected at low temperatures. Also, Olsson et al. [3] showed that approximately 30% of the Pt surface is covered by NO at 240 °C, and the coverage decreases with an increase in temperature. However, values of the coverage at temperatures lower than 240 °C were not provided. If the coverage of NO is neglected, Eq. (4.20) reduces to

$$R_{v,NO\_ox} = \frac{k_{f2} K_1 K_3 X_{NO,s} X_{O_2,s}}{K_4 X_{NO_2,s}}\left[1 - \left(\frac{X_{NO_2,s}}{K_{eq}\sqrt{X_{O_2,s}} X_{NO,s}}\right)^2\right] \tag{4.22}$$

Eq. (4.22) was used to predict the dependence of steady-state NO conversion on the catalyst temperature (Fig. 15). At low temperatures, the model does not capture the experimental trends; this suggests that the assumption of a negligible NO coverage is not valid at these temperatures. Thus, the global rate expression is an improvement over existing global models from the literature. The NO oxidation model given by Eq. (4.20) has also been used to correctly predict the transient outlet NO_x concentration profiles during the lean phase of the NSR cycle, and the results are reported elsewhere [37].

We made an attempt to find the order of NO oxidation reaction with respect to NO_2 concentration by varying the concentration of NO_2 and measuring the steady-state reaction rates. The NO_2 concentration was varied in a random order to prevent systematic errors. However, the reproducibility of the data was unsatisfactory when the catalyst was subjected to a high NO_2 concentration, before repeating the experiment for a low inlet NO_2 concentration. This is probably because of the irreversible catalyst poisoning due to the formation of oxides at a high inlet NO_2 concentration. However, in a recent study, Mulla et al. [11] reported a negative order with respect to NO_2 for the steady-state NO oxidation reaction over a Pt/Al_2O_3 catalyst. We used the global rate expression given by Eq. (4.20) to study the effect of inlet NO_2 concentration on the

Table 8
Values of global reaction parameters used in the simulations.

Parameter	Numerical value (mol/m^3 washcoat s)	Parameter	Numerical value (kJ/mol)
A_{b1}	1.27×10^{16}	E_{b1}	106.9
A_{f2}	1.41×10^{5}	E_{f2}	0.0
A_{b2}	1.74×10^{13}	E_{b2}	80.0
A_{f5}	4.94×10^{18}	E_{f5}	80.0
A_{b5}	1.0×10^{22}	E_{b5}	209.4
		E_{b3}	44.9

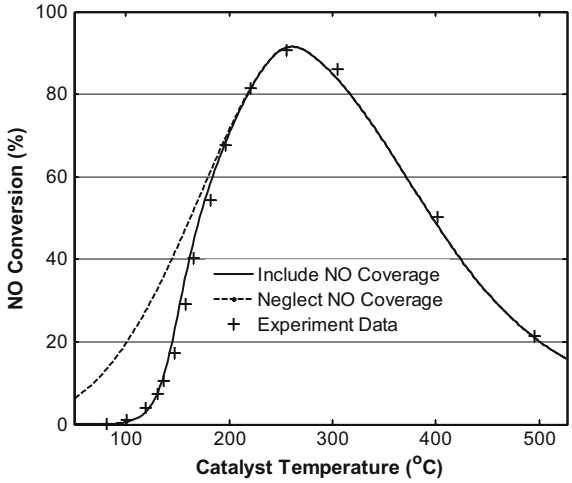

Fig. 15. Comparison of model predicted and experimental NO conversion for various catalyst temperatures with and without neglecting NO coverage on the catalyst surface (inlet NO = 482 ppm, O_2 = 5%, Pt/Al_2O_3 catalyst).

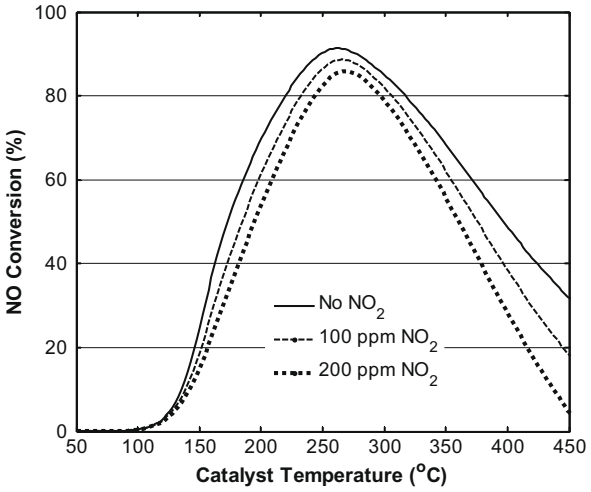

Fig. 16. Model predicted effect of inlet NO_2 concentration on NO conversion (inlet NO = 500 ppm, O_2 = 5%, Pt/Al_2O_3 catalyst).

predicted NO conversion for a feed consisting of 500 ppm NO and 5% O_2. The simulation results are presented in Fig. 16 and it is observed that the model is able to predict the inhibition effect of NO_2 on the NO oxidation rates.

The effect of inlet NO_2 concentration on the conversion of NO_2 during its decomposition is predicted using Eq. (4.20) and the results are shown in Fig. 17. It is observed that at steady state, the model predicts a decrease in NO_2 conversion with increase in inlet NO_2 concentration. The predicted trends are similar to the experimentally observed NO_2 conversion trends after 90 min (Fig. 13). As discussed earlier, the steady-state experimental data reported in this work may be close to the steady-state but might not be the "true" steady-state for the intermediate temperature range (180–350 °C). Hence, strictly speaking, the model predicted values should be compared with the experimental values for this temperature range with some caution. However, for practical purposes, the global kinetic model proposed in the current work is able to predict the "pseudo-steady" experimental data for a wide temperature range. More accurate predictions for the entire temperature range would require a detailed elementary kinetic model and should include the effect of O_2 and NO_2 on the formation of chemisorbed oxygen and Pt oxides, among other surface reactions. However, this is beyond the scope of the current work but is a topic of future investigation.

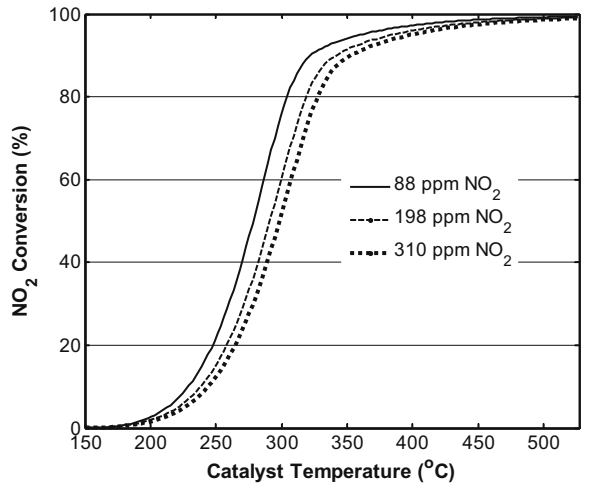

Fig. 17. Model predicted effect of inlet NO_2 concentration on steady-state NO_2 conversion for various catalyst temperatures (Pt/Al_2O_3 catalyst).

5. Summary and conclusions

Steady-state modeling and experimental studies have been performed to elucidate the kinetics of the NO oxidation reaction. The studies highlight the challenges of modeling the system due to the coupled NO oxidation, NO_x storage, and catalyst poisoning effects. Hence, experiments were performed for various inlet feeds and inlet conditions to study the individual processes, i.e. NO oxidation, NO_2 decomposition, NO_2 storage, and catalyst poisoning.

NO oxidation experiments in the kinetically controlled regime were performed on $Pt/BaO/Al_2O_3$ and an activation energy of 81.8 kJ/mol was found. Experiments with Pt/Al_2O_3 and $Pt/BaO/Al_2O_3$ demonstrate that a steady-state is never truly achieved in the system. Transient experiments for various catalyst pretreatments were performed on Pt/Al_2O_3 to elucidate the cause of the slow decrease in NO oxidation activity. These experiments indicate that NO_2, because of its highly oxidizing nature, results in the formation of Pt oxides/chemisorbed oxygen, which reduces the catalyst activity. The presence of O_2 also decreases the catalyst activity, but the poisoning effect of O_2 is much less than that of NO_2. Chemisorbed oxygen can react with NO resulting in the restoration of the activity, but the formation of Pt oxides results in the loss of activity, which is not regained during the oxidation reaction. An analysis of the exit N concentration reveals that NO_x storage plays an insignificant role in the activity decrease. In addition to the poisoning effects of NO_2 and O_2, a comparison of NO conversion in the presence of varied concentrations of NO_2 shows a decrease in NO conversion with an increase in inlet NO_2 concentration, confirming an inhibitory effect of NO_2 on the NO oxidation reaction. A comparison of Pt/Al_2O_3 and $Pt/BaO/Al_2O_3$ catalyst shows that Pt/Al_2O_3 catalysts are more active than $Pt/BaO/Al_2O_3$ for the NO oxidation reaction, which could be due to the blocking of Pt sites by the BaO storage phase and/or to a higher amount of Pt oxide formation on $Pt/BaO/Al_2O_3$ as compared to Pt/Al_2O_3.

The disproportionation pathway of NO_2 storage was experimentally confirmed by flowing NO_2 over $Pt/BaO/Al_2O_3$ catalyst at a low temperature (100 °C). However, at high temperatures, the formation of NO occurs by storage as well as decomposition of NO_2. Since NO_2 results in the formation of NO at all temperatures, NO formation should not be neglected in modeling of the NO oxidation reaction. NO_2 decomposition experiments for various inlet NO_2 concentrations show the decrease in outlet NO concentration with an increase in inlet NO_2 concentration, which again confirms the oxidizing effect of NO_2 in reducing the catalyst activity.

Microkinetic analysis of the NO oxidation reaction was performed and NO coverage was found to be important at low temperatures, which is neglected in existing literature models. Parametric sensitivity analysis of the microkinetic scheme shows O_2 adsorption/desorption as the rate-determining step for the NO oxidation and NO_2 decomposition reactions. Based on the microkinetic studies, a global kinetic model is proposed which includes the inhibitory effect of NO_2 on the NO oxidation reaction. The model predicts the experimentally observed dependence of steady-state NO conversion on temperature over a wide temperature range. It also predicts the decrease in NO and NO_2 conversions for the NO oxidation and NO_2 decomposition reactions, respectively, with an increase in inlet NO_2 concentration. However, for predicting the transient data, a detailed elementary kinetic model should be used, which includes the storage effects and the effect of O_2 and NO_2 on the formation of chemisorbed oxygen and Pt oxides, besides other surface reactions. This is the subject of an ongoing investigation.

Acknowledgments

The work reported was supported by Ford Motor Company and the US DOE National Energy Technology Laboratory (DE-FC26-05NT42630). We also acknowledge BASF Catalysts LLC for providing the catalysts used in this study. One of the authors (Divesh Bhatia) acknowledges the support of Ford Motor Company during his summer internship in the Ford Research Laboratories in Dearborn, Michigan. The authors thank Professor Randall Meyer of the University of Illinois at Chicago for his useful comments on an earlier version of the manuscript.

References

[1] S. Erkfeldt, E. Jobson, M. Larrson, Top. Catal. 16/17 (1–4) (2001) 127.
[2] W.S. Epling, L.E. Campbell, A. Yezerets, N.W. Currier, J.E. Parks II, Catal. Rev. 46 (2) (2004) 163.
[3] L. Olsson, H. Persson, E. Fridell, M. Skoglundh, B. Andersson, J. Phys. Chem. B 105 (2001) 6895.
[4] N.W. Cant, I.O.Y. Liu, M.J. Patterson, J. Catal. 243 (2006) 309.
[5] I. Nova, L. Lietti, L. Castoldi, E. Tronconi, P. Forzatti, J. Catal. 239 (2006) 244.
[6] L. Olsson, E. Fridell, J. Catal. 210 (2002) 340.
[7] R. Marques, P. Darcy, P.D. Costa, H. Mellottee, J.M. Trichard, G.D. Mariadassou, J. Mol. Catal. A: Chem. 221 (2004) 127.
[8] R.L. Muncrief, P. Khanna, K.S. Kabin, M.P. Harold, Catal. Today 98 (2004) 393.
[9] S.S. Mulla, N. Chen, W.N. Delgass, W.S. Epling, F.H. Ribeiro, Catal. Lett. 100 (3–4) (2005) 267.
[10] S.S. Mulla, N. Chen, L. Cumaranatunge, W.N. Delgass, W.S. Epling, F.H. Ribeiro, Catal. Today 114 (2006) 57.
[11] S.S. Mulla, N. Chen, L. Cumaranatunge, G.E. Blau, D.Y. Zemlyanov, W.N. Delgass, W.S. Epling, F.H. Ribeiro, J. Catal. 241 (2006) 389.
[12] W. Hauptmann, A. Drochner, H. Vogel, M. Votsmeier, J. Gieshoff, Top. Catal. 42–43 (2007) 157.
[13] L. Olsson, B. Westerberg, H. Persson, E. Fridell, M. Skoglundh, B. Andersson, J. Phys. Chem. B 103 (1999) 10433.
[14] R.D. Clayton, M.P. Harold, V. Balakotaiah, C.Z. Wan, Appl. Catal. B (2009), doi:10.1016/j.apcatb.2009.04.029.
[15] D. Bhatia, M.P. Harold, V. Balakotaiah, Chem. Eng. Sci. 64 (2009) 1544.
[16] K. Ramanathan, V. Balakotaiah, Chem. Eng. Sci. 58 (2003) 1381.
[17] M. Kubicek, ACM Trans. Math. Softw. 2 (1) (1976) 98.
[18] L.S. Mukadi, R.E. Hayes, Comput. Chem. Eng. 26 (2002) 439.
[19] K. Ramanathan, D.H. West, V. Balakotaiah, Ind. Eng. Chem. Res. 43 (2004) 4668.
[20] J.H. Lee, H.H. Kung, Catal. Lett. 51 (1998) 1.
[21] I. Nova, L. Castoldi, L. Lietti, E. Tronconi, P. Forzatti, F. Prinetto, G. Ghiotti, J. Catal. 222 (2002) 377.
[22] W.S. Epling, J.E. Parks, G.C. Campbell, A. Yezerets, N.W. Currier, L.E. Campbell, Catal. Today 96 (2004) 21.
[23] K.S. Kabin, P. Khanna, R.L. Muncrief, V. Medhekar, M.P. Harold, Catal. Today 114 (2006) 72.
[24] R.D. Clayton, M.P. Harold, V. Balakotaiah, AIChE J. 55 (3) (2009) 687.
[25] A.D. Smeltz, R.B. Getman, W.F. Schneider, F.H. Ribeiro, Catal. Today 136 (2008) 84.
[26] H. Yoshida, Y. Yazawa, N. Takagi, A. Satsuma, T. Tanaka, S. Yoshida, T. Hattori, J. Synchrotron Rad. 6 (3) (1999) 471.
[27] J. Segner, W. Vielhaber, G. Ertl, Isr. J. Chem. 22 (1982) 375.
[28] D.H. Parker, B.E. Koel, J. Vac. Sci. Technol. A 8 (3) (1990) 2585.
[29] R.B. Getman, W.F. Schneider, A.D. Smeltz, W.N. Delgass, F.H. Ribeiro, Phys. Rev. Lett. 102 (2009) 076101-1.
[30] P.R. Norton, J.A. Davies, T.E. Jackman, Surf. Sci. 122 (1) (1982) L593.
[31] A. Lindholm, N.W. Currier, E. Fridell, A. Yezerets, L. Olsson, Appl. Catal. B 75 (2007) 78.
[32] L. Olsson, R.J. Blint, E. Fridell, Ind. Eng. Chem. Res. 44 (9) (2005) 3021.
[33] J. Xu, V. Balakotaiah, M.P. Harold, Appl. Catal. B 89 (1–2) (2009) 73.
[34] B. Shan, N. Kapur, J. Hyun, L. Wang, J.B. Nicholas, K. Cho, J. Phys. Chem. C 113 (2009) 710.
[35] A.C. Luntz, J. Grimblot, D.E. Fowler, Phys. Rev. B 39 (17) (1989) 12903.
[36] T. Zambelli, J.V. Barth, J. Wintterlin, G. Ertl, Nature 390 (1997) 495.
[37] D. Bhatia, R.D. Clayton, M.P. Harold, V. Balakotaiah, Catal. Today, doi:10.1016/j.cattod.2009.07.024.